Popular Summary of

Response of the Antarctic Stratosphere to two types of El Niño Events

submitted to Journal of the Atmospheric Sciences, July 2010

M.M. Hurwitz [1], **P.A. Newman** [2], **L.D. Oman** [2] and **A.M. Molod** [3]

1 *NASA Postdoctoral Program, NASA Goddard Space Flight Center, Greenbelt, MD, USA*

2 *NASA Goddard Space Flight Center, Greenbelt, MD, USA*

3 *Goddard Earth Sciences and Technology Center, University of Maryland, Baltimore County, Baltimore, MD, USA*

Conventional El Niño events are characterized by warmer than average sea surface temperatures in the equatorial eastern Pacific Ocean and by an eastward shift in atmospheric convection from Asia toward the central Pacific. The largest El Niño event in recent decades occurred in 1997/1998. The El Niño signal propagates polewards and upwards as large-scale atmospheric waves, leading to unusual weather worldwide and changing conditions in the stratosphere. While the Arctic stratosphere warms in response to these conventional or "cold tongue" type of El Niño events, the Antarctic stratosphere is unaffected.

Recently, a second type of El Niño event has been identified. During "warm pool" El Niño events, sea surface temperatures in the central Pacific are warmer than average. This study identifies a robust warming of the Antarctic stratosphere in Southern Hemisphere spring and summer, in response to "warm pool" El Niño events, using atmospheric data from 1979 to 2009. The Antarctic warming associated with "warm pool" El Niño events is most pronounced when these events are coincident with westward winds in the tropical lower and middle stratosphere. Westward winds may enhance wave activity in the subtropical troposphere and/or push wave energy toward polar latitudes. Because of the small number of observed El Niño events, model experiments will be required to better understand how tropical winds affect the Antarctic response to "warm pool" El Niño events.

Response of the Antarctic Stratosphere to two types of El Niño Events

M. M. Hurwitz [1], **P. A. Newman** [2], **L. D. Oman** [2] and **A. M. Molod** [3]

1 NASA Postdoctoral Program, NASA Goddard Space Flight Center, Greenbelt, MD, USA

2 NASA Goddard Space Flight Center, Greenbelt, MD, USA

3 Goddard Earth Sciences and Technology Center, University of Maryland, Baltimore County, Baltimore, MD, USA

Corresponding author information

Email address: margaret.m.hurwitz@nasa.gov

Mailing address: NASA Goddard Space Flight Center
Code 613.3
Greenbelt, MD
USA 20771

Abstract

This study is the first to identify a robust El Niño/Southern Oscillation (ENSO) signal in the Antarctic stratosphere. El Niño events are classified as either conventional "cold tongue" events (positive SST anomalies in the Niño 3 region) or "warm pool" events (positive SST anomalies in the Niño 4 region). The ERA-40, NCEP and MERRA meteorological reanalyses are used to show that the Southern Hemisphere stratosphere responds differently to these two types of El Niño events. Consistent with previous studies, "cold tongue" events do not impact temperatures in the Antarctic stratosphere. During "warm pool" El Niño events, the poleward extension and increased strength of the South Pacific Convergence Zone (SPCZ) favor an enhancement of planetary wave activity during the SON season. On average, these conditions lead to higher polar stratospheric temperatures and a weakening of the Antarctic polar jet in November and December, as compared with neutral ENSO years. The phase of the quasi-biennial oscillation (QBO) modulates the stratospheric response to "warm pool" El Niño events: the strongest planetary wave driving events are coincident with the easterly phase of the QBO.

1 Introduction

El Niño/Southern Oscillation (ENSO) has a stratospheric signature in both the tropics and in the Arctic. In the tropics, the lower stratospheric temperature response to ENSO has the opposite sign as that in the troposphere, i.e. a cooling associated with ENSO warm phase (El Niño) events (Calvo Fernandez et al., 2004; Garcia-Herrera et al., 2006; Free and Seidel, 2009). This tropical lower stratospheric cooling reflects the strengthening of the upwelling branch of the Hadley cell. Using both observations and a chemistry-climate model (CCM), Randel et al. (2009) showed that increased tropical upwelling during El Niño events leads to coherent variability in tropical ozone and temperature.

El Niño events have been shown to weaken the Northern Hemisphere polar vortex. El Niño-related warming of the Arctic stratosphere has been identified in observational (Bronnimann et al., 2004; Free and Seidel, 2009) and modeling studies (Sassi et al., 2004; Manzini et al., 2006; Cagnazzo et al., 2009). Warming of the Arctic stratosphere is a response to increased planetary wave driving: Garfinkel and Hartmann (2008) showed that the extratropical tropospheric teleconnections produced during El Niño events weaken the Arctic vortex, leading to higher stratospheric temperatures during the NH winter season. The phase of the quasi-biennial oscillation (QBO) (Garfinkel and Hartmann, 2007; Bronnimann, 2007) and volcanic activity (Randel et al., 2009) modulate this response. The Arctic vortex is weakest in years when El Niño events coincide with the easterly phase of the QBO (Garfinkel and Hartmann, 2007).

Previous studies of the stratospheric response to ENSO have considered a single type of El Niño event. The sea surface temperature (SST) anomaly pattern associated with these events, a band of positive SST anomalies spanning the eastern Pacific, was identified by Rasmusson and Carpenter (1982) and was termed a "cold tongue" El Niño event (hereafter CT El Niño) by Kug et al. (2009). The SST and precipitation anomalies associated with CT El Niño events develop during the June-July-August (JJA) and September-October-November (SON) seasons, peak in December-January-February (DJF), and decay in the March-April-May (MAM) season. The multivariate ENSO index (MEI; www.esrl.noaa.gov/psd/people/klaus.wolter/MEI), Niño 3 and Niño 3.4 indices (www.cpc.noaa.gov/data/indices) capture this leading mode of variability in the tropical Pacific (Calvo Fernandez et al., 2004; Ashok et al., 2007) and maximize during CT El Niño events, when SST anomalies and convective activity in the eastern equatorial Pacific are unusually high. The two largest CT El Niño events of the satellite era occurred in 1982/1983 and 1997/1998 (Kug et al., 2009).

Recent literature recognizes a second type of El Niño event. These events have been referred to as "dateline El Niño" (Larkin and Harrison, 2005), "El Nino Modoki" (Ashok et al., 2007) and "warm pool El Niño" (Kug et al., 2009) (hereafter WP El Niño). WP El Niño events capture the secondary mode of variability in tropical Pacific SSTs: positive SST anomalies in the tropical central Pacific, and negative SST anomalies in the western and eastern tropical Pacific (Ashok et al., 2007). SST and precipitation anomalies maximize in the SON and DJF seasons (Kug et al., 2009; Yu and Kim, 2010). The largest observed WP El Niños occurred in the early 1990s.

The two types of El Niño events can be distinguished not only by the region in which SST anomalies are greatest, but also by the relative position and strength of the South Pacific Convergence Zone (SPCZ). Vera et al. (2004) found that the extratropical component of the SPCZ is stronger and extends further south in WP El Niño-like events as compared with either CT El Niño-like or ENSO neutral events. The same authors found relative increase in planetary wave activity in the south central Pacific in response to all El Niño events, and furthermore, identified a Rossby wave source centered at approximately 20°S, 240°E in El Niño events with enhanced SPCZ activity (WP El Niño-like) relative to El Niño events with suppressed SPCZ activity (CT El Niño-like).

While the planetary wave response to CT El Niño modulates conditions in the Arctic stratosphere (Garfinkel and Hartmann, 2008), this paper shows that an analogous enhancement in wave activity during WP El Niño events affects conditions in the Antarctic stratosphere. In particular, differences between the SH wave response to WP El Niño and CT El Niño may explain much of the interannual variability in the strength of the Antarctic vortex. In Section 2, atmospheric datasets are defined and El Niño events are categorized. In Section 3, tropospheric stationary wave patterns, eddy heat flux, stratospheric temperature and winds are used to illustrate the atmospheric response to El Niño events, as well as the modulation of this response by the QBO. Section 4 provides a summary of the results and a brief discussion.

2 Methods

2.1 Identification of El Niño events and QBO phase

In this study, El Niño events are identified using two climate indices. The Niño 3 index (www.cpc.noaa.gov/data/indices) measures SST anomalies in the eastern equatorial Pacific Ocean (the Niño 3 region; 5°S-5°N, 210-270°E). The Niño 4 index measures SST anomalies in the central equatorial Pacific (the Niño 4 region; 5°S-5°N, 160-210°E). In this study, WP El Niño events are identified when SON seasonal mean Nino 4 anomalies exceed one standard deviation from the 1971-2000 mean (Figure 1, top panel). CT El Niño events are identified when SON mean Niño 3 anomalies exceed one standard deviation from the 1971-2000 mean, and, are larger than the corresponding Niño 4 anomalies (Figure 1, second panel). Note that WP El Niño events appear as secondary peaks in the Niño 3 timeseries. Note also that the Niño 3 standard deviation is larger than the Niño 4 standard deviation; that is, the magnitudes of the positive SST anomalies that define a WP El Niño event are smaller than those that define a CT El Niño event. Neutral ENSO years are defined as those when the SON and DJF mean Niño 3 and Niño 4 indices are both between -0.7 and 0.7. Table 1 specifies years in which the above criteria are met. Kug et al. (2009) used the SONDJF seasonal mean to select a slightly different set of WP and CT El Niño events; also, the authors defined a "mixed" type of El Niño event in which the maximum area of SST anomalies is located between the Niño 3 and Niño 4 regions.

A third index characterizes the phase of the quasi-biennial oscillation (QBO). Following Garfinkel and Hartmann (2008), this index is calculated by averaging 50 hPa zonal winds between 10°S and 10°N from November through February (i.e., the austral summer season following each SON season). QBO easterly years (QBO-E) are defined when the QBO index is larger than 3.3 m s^{-1} and QBO

163 westerly years (QBO-W) are defined when the QBO index is less
164 than -3.3 m s^{-1} (Figure 1, third panel). Easterly QBO years are
165 denoted with star symbols in Table 1; years when WP El Niño
166 coincides with the easterly phase of the QBO are denoted as thick
167 blue stars in Figure 1 (third panel).
168
169 **2.2 Atmospheric Datasets**
170 Various atmospheric datasets are used to assess the atmospheric
171 response to the two types of El Niño events as defined in Section
172 2.1. Monthly mean precipitation is taken from the Global
173 Precipitation Climatology Project (GPCP) merged precipitation
174 dataset, version 2.1 (Adler et al., 2003; Bolvin et al., 2009).
175 Data are available from 1979 through 2007, with 2.5° x 2.5°
176 horizontal resolution. Three meteorological reanalyses are used
177 to calculate streamfunction, heat flux, temperature and zonal
178 wind diagnostics. Given the small number of observed El Niño
179 events since 1979, similarities in the El Niño response between
180 two or more reanalysis datasets will increase the robustness of
181 the results. Also, multiple reanalyses will test the sensitivity
182 of the results to the number and type of events included in the
183 analysis.
184
185 The European Centre for Medium-Range Weather Forecasts' 40-year
186 meteorological reanalysis (ERA-40) (Uppala et al., 2005) has
187 vertical coverage up to 1 hPa, and for this study, is
188 interpolated to a 2.5° x 2.5° horizontal grid. The 1979-2001
189 period is used in this analysis.
190
191 The Modern Era Retrospective-Analysis for Research and
192 Applications (MERRA) is a reanalysis dataset based on an
193 extensive set of satellite observations and on the Goddard Earth

Observing System Data Analysis System, Version 5 (GEOS-5) (Bosilovich et al., 2008). Currently, the MERRA reanalysis extends from 1979 through 2009. The MERRA reanalysis has vertical coverage up to 0.1 hPa, and for this study, 1.25° x 1.25° horizontal resolution.

The National Centers for Environmental Prediction-US Department of Energy (NCEP-DOE) reanalysis-2 product (Kanamitsu et al., 2002) covers the period from 1979 through 2009. The NCEP reanalysis has 2.5° x 2.5° horizontal resolution and vertical coverage up to 10 hPa.

3 Results

3.1 Southern Hemisphere response to WP El Niño and CT El Niño events

In this section, observed precipitation, horizontal winds, eddy heat flux and temperature fields are used to show that the strength and position of the SPCZ controls the SH stratospheric response to El Niño events.

The strength and position of the SPCZ are largely controlled by the phase of ENSO (Juillet-Leclerc et al., 2006), and furthermore, by the type of El Niño event. Figure 2 shows GPCP precipitation differences, in WP El Niño and CT El Niño events relative to an ENSO neutral composite, in the SPCZ region. There is more precipitation associated with the SPCZ, which extends diagonally from the northwest to the southeast corner of each plot, during both types of El Niño events than in ENSO neutral years. In WP El Niño events (Figure 2a), there is a coherent increase in precipitation of 0.5-1 mm day^{-1} at the southeastern edge of the SPCZ. This region of increased precipitation

225 coincides with the location of the largest correlations between
226 precipitation and October/November mid-latitude heat flux at 100
227 hPa (Figure 3).
228
229 El Niño events trigger a planetary wave response in the SH. Vera
230 et al. (2004) found that the intensification and southeastward
231 extension of SPCZ activity strengthened the local overturning
232 circulation, leading to a relative Rossby wave source in the
233 south central Pacific in WP-like as compared with CT-like El Niño
234 events. This analysis will reproduce the results of Vera et al.
235 (2004) using WP and CT El Niño events, as defined in Section 2.1.
236 In Figure 4, 250 hPa SON streamfunction differences from an ENSO
237 neutral composite illustrate the planetary wave responses to both
238 types of El Niño events. Each panel of Figure 4 shows a
239 wavetrain response to El Niño: Negative streamfunction
240 differences in the subtropics, close to the dateline (region
241 denoted by A in Figure 4c), positive streamfunction differences
242 at mid-latitudes (region B), and negative streamfunction
243 differences around 240°E, 60°S (region C). The red arrows in
244 Figures 4a and 4b indicate the approximate propagation direction
245 of the wavetrains. The region A and B differences are
246 statistically significant in both types of El Nino events, and in
247 all three reanalyses. Region C differences are statistically
248 significant in the case of WP El Niño (Figures 4a, 4c and 4e) but
249 are not statistically significant in CT El Niño (Figures 4b, 4d
250 and 4f). The fourth panel in Figure 1 shows a timeseries of 250
251 hPa streamfunction in region C; note that the lowest values are
252 concurrent with WP El Niño events. This evidence suggests that
253 there is a stronger planetary wave response to WP El Niño events
254 than to CT El Niño events, consistent with Vera et al. (2004).
255

Eddy heat flux is used to quantify the amount of planetary wave energy entering the stratosphere during El Niño and ENSO neutral events. Eddy heat flux ($\overline{v'T'}$) at 100 hPa, averaged between 40°S and 80°S, has been used to diagnose planetary wave driving in chemistry-climate model validation studies (Austin et al., 2003; Eyring et al., 2006). October/November eddy heat flux at 100 hPa will be the focus of this study, as previous work has shown that it plays an important role in the timing of the breakup of the Antarctic vortex (Hurwitz et al., 2010). Table 2 shows the mean eddy heat flux magnitudes in each of the ENSO cases, and for each of the reanalyses. For the MERRA and NCEP reanalyses, mean eddy heat flux is shown both for the ERA-40 period (1979-2001) and for 1979-2009. Eddy heat flux values are broadly consistent amongst the three reanalyses (see also Figure 1, fifth panel) and are not sensitive to the length of the timeseries used in the analysis. Note, however, that eddy heat flux is largest in the WP El Niño cases, and furthermore, larger in the 1979-2001 period as compared with the 1979-2009 period. Variability among WP El Niño events is roughly twice as large as that between CT El Niño and ENSO neutral events (see discussion in Section 3.2).

Newman et al. (2001) identified a positive relationship between mid-latitude eddy heat flux at 100 hPa and polar temperatures at 50 hPa, with a roughly one-month lag. Given the relatively larger October/November eddy heat flux values in WP El Niño events as compared with CT El Niño and ENSO neutral events (Table 2), the November/December stratospheric temperature response to WP El Niño events would be expected to be larger from that of CT El Niño events. Figure 5 shows mean November/December temperature differences in the WP El Niño and CT El Niño composites, as compared with neutral ENSO years. At polar

latitudes, WP El Niño events (Figures 5a, 5c and 5e) warm the tropical upper troposphere and lower stratosphere and cool the upper stratosphere. The lower stratospheric warming response is statistically significant in ERA-40 (3-5 K) but not in MERRA or NCEP. The upper stratospheric cooling (1-2 K in MERRA; see Figure 5c) is a wave filtering effect (Hurwitz et al., 2010): in WP El Niño events, heat flux is higher and the Antarctic vortex breaks up earlier. Summertime easterly winds do not allow planetary wave propagation, leading to lower temperatures. During CT El Nino events (Figures 5b, 5d and 5f), consistent with previous observational studies (Free and Seidel, 2009; Randel et al., 2009), none of the reanalyses show a statistically significant temperature response in the Antarctic lower stratosphere.

3.2 QBO influence on the response to WP El Niño events

The response of the Antarctic stratosphere to WP El Niño events is systematically different from that to CT El Niño events. However, the relative increases in heat flux and polar lower stratospheric temperatures during WP El Niño events are not statistically different from ENSO neutral events. The high degree of variability amongst WP El Niño events may be related to the phase of the QBO.

In the Arctic lower stratosphere, the largest warming response to CT El Niño is seen in years when the phase of the QBO is easterly (Calvo Fernandez et al., 2004; Manzini et al., 2006). The Antarctic lower stratosphere responds analogously. Of WP El Niño events, eddy heat flux is larger in years when the QBO is easterly than in years when winds are either weak or westerly (Table 3); differences between the two QBO groupings are

318 significant at the 95% level in all three reanalyses.
319 Conversely, in ENSO neutral years, the QBO phase makes no
320 difference to the magnitude of the October/November eddy heat
321 flux. The sensitivity of CT El Niño events to QBO phase cannot
322 be assessed, as all three observed CT El Niño events coincide
323 with weak equatorial zonal winds at 50 hPa.
324
325 The NCEP reanalysis is used to examine the temperature response
326 to WP El Niño events, as a function of QBO phase, as its
327 timeseries are long enough to sample of each of the QBO and ENSO
328 cases. The MERRA reanalysis yields very similar results.
329 Figures 6a and 6b show temperature differences between WP El Niño
330 events, partitioned by QBO phase, and the ENSO neutral composite.
331 At high latitudes, a warming of 3-5 K is seen in easterly QBO
332 years (Figure 6a) whereas there is no significant warming in
333 years when the QBO is either neutral or westerly (Figure 6b).
334
335 In the Antarctic stratosphere, the zonal wind response to El Niño
336 events is consistent with the temperature response. The relative
337 warming of the lower Antarctic stratosphere during WP El Niño
338 events reduces the meridional temperature gradient, and by the
339 thermal wind balance, weakens the polar jet. The largest wind
340 differences from the ENSO neutral composite are seen in WP El
341 Niño events coincident with QBO-E (note the easterly winds at 50
342 hPa at the equator in Figure 6c). In the NCEP reanalysis, there
343 are statistically significant negative zonal wind differences of
344 up to 7 m s^{-1} in the lower and middle stratosphere at
345 approximately 60°S (Figure 6c). This jet weakening is
346 approximately twice as large as that seen in the WACCM model in
347 the Arctic stratosphere in January (Taguchi, 2010), in ENSO warm
348 phase as compared with cold phase events. Consistent with the

negligible temperature differences seen in Figure 5, the Antarctic jet does not weaken in response to CT El Niño events,

4 Summary and Discussion

This study examined the response of the Antarctic stratosphere to two types of El Niño events: warm pool (WP) El Niño and cold tongue (CT) El Niño. WP El Niño events are characterized by positive SST anomalies in the equatorial central Pacific (i.e., the Niño 4 region) during austral spring and summer. This analysis found that the Niño 4 index is a better indicator of the SH dynamical response to El Niño than are indices that favor the eastern Pacific. The Niño 3, Niño 3.4 and MEI indices have been used in previous studies to identify the stratospheric signature of CT El Niño events in the tropics and in the Arctic; however, these indices have failed to identify an El Niño response in the Antarctic stratosphere. Thus, evaluation of the global impact of ENSO on the stratosphere requires measures of SST changes in both the eastern (Niño 3) and central equatorial Pacific (Niño 4) regions.

The strength and poleward extension of the SPCZ during the SON season largely determine the SH stratospheric response to ENSO. While SPCZ activity increases during both types of El Niño events, precipitation is significantly enhanced in the southeastern part of the SPCZ during WP El Niño events. Both types of El Niño events generated a planetary wave response in the SH troposphere, but again, this wave response extended further poleward during WP El Niño events than during CT El Niño events. As a result, SH planetary wave driving in October and November (specifically, mid- to high latitude heat flux at 100

379 hPa) was stronger during WP El Niño events, compared with both CT
380 El Niño events and ENSO neutral years.
381
382 During WP El Niño events, enhanced planetary wave activity warmed
383 the Antarctic upper troposphere and lower stratosphere and
384 weakened the stratospheric polar jet. The Antarctic response to
385 WP El Niño appears to be modulated by the phase of the QBO: a 3-5
386 K warming was seen in QBO easterly phase events whereas there was
387 no significant warming in years with a weak or westerly QBO.
388 Following the Holton and Tan (1980) mechanism, the easterly phase
389 of the QBO may confine lower stratospheric planetary wave-
390 breaking to middle and high latitudes, weakening the Antarctic
391 vortex. However, during WP El Niño events, the strength of the
392 SPCZ is highly dependent on the phase of the QBO, suggesting that
393 a tropical mechanism may be involved. Collimore et al. (2003)
394 argue that the phase of the QBO modulates the tropopause height
395 and thus the height of deep convection in the tropics. These
396 authors found a strengthening of convective activity in the SPCZ
397 region during austral spring, in QBO-E relative to QBO-W years,
398 possibly explaining the QBO modulation of the SH stratospheric
399 response to WP El Niño events. Compared with the 2-4 K warming
400 of the Arctic lower stratosphere during CT El Niño events, as
401 found by Free and Seidel (2009), the warming of the Antarctic
402 lower stratosphere during WP El Niño events was comparable during
403 easterly QBO years but weaker on average. Coupled ocean-
404 atmosphere model simulations predict that the pattern of SST
405 trends will favor WP El Niño events in future (Yeh et al., 2009;
406 Xie et al., 2010); thus, ENSO-related warming of the Antarctic
407 lower stratosphere may offset some of the direct radiative
408 cooling by greenhouse gases.
409

While WP El Niño events have a significant impact on temperature, they have a negligible impact on polar ozone. WP El Niño events reach maturity in austral spring and summer (Kug et al., 2009), after the formation of the ozone hole. Compared with ENSO neutral years, ozone differences in the Antarctic lower stratosphere were negligible in both WP El Niño and CT El Niño events.

The ERA-40, MERRA and NCEP reanalyses were in agreement when the same time periods were compared. That is, the different horizontal and vertical resolutions of the three reanalysis datasets did not affect the results. However, the stratospheric response to WP El Niño events was dependent on the time period analyzed: the WP El Niño events after 2001 mainly occurred in westerly or neutral QBO years, reducing the e.g., mean temperature response to WP El Niño events in MERRA and NCEP (1979-2009) as compared with ERA-40 (1979-2001).

One shortcoming of using meteorological reanalyses to diagnose the stratospheric response to El Niño events is the small number of such events that occurred between 1979 and 2009. The statistical significance of the results was lacking in some cases (i.e., the temperature response to WP El Niño events in the MERRA and NCEP reanalyses). Time-slice simulations, with repeating El Niño-like boundary conditions, would greatly increase the sample size and better separate the WP El Niño and CT El Niño signals from the variability between events of the same type.

Acknowledgements

439 MMH is supported by an appointment to the NASA Postdoctoral
440 Program at Goddard Space Flight Center, administered by Oak Ridge
441 Associated Universities through a contract with NASA.
442

References

Adler, R. F., and Coauthors, 2003: The version-2 global precipitation climatology project (GPCP) monthly precipitation analysis (1979-present). *J. Hydrometeorol.*, **4**, 1147-1167.

Ashok, K., S. K. Behera, S. A. Rao, H. Weng, and T. Yamagata, 2007: El Niño Modoki and its possible teleconnections. *J. Geophys. Res.*, **112**, C11007, doi:10.1029/2006JC003798.

Austin, J., and Coauthors, 2003: Uncertainties and assessments of chemistry-climate models of the stratosphere. *Atmos. Chem. Phys.*, **3**, 1-27.

Bolvin, D. T., R. F. Adler, G. J. Huffman, E. J. Nelkin and J. P. Poutiainen, 2009: Comparison of GPCP monthly and daily precipitation estimates with high-latitude gauge observations. *J. Appl. Meteor. Climatol.*, **48**, 1843-1857.

Bronnimann, S., 2007: The impact of El Niño-Southern Oscillation on European climate. *Rev. Geophys.*, **45**, RG3003, doi:10.1029/2006RG000199.

Bronnimann, S., J. Luterbacher, J. Staehelin, T. M. Svendby, G. Hansen, and T. Svene, 2004: Extreme climate of the global troposphere and stratosphere in 1940-42 related to El Niño. *Nature*, **431**, 971-974, doi:10.1038/nature02982.

Bosilovich, M., 2008: NASA'S modern era retrospective-analysis for research and applications: integrating earth observations. *Earthzine*, Sep. 26.

Cagnazzo, C., and Coauthors, 2009: Northern winter stratospheric temperature and ozone response to ENSO inferred from an ensemble of Chemistry Climate Models. *Atmos. Chem. Phys.*, **9**, 8935-8948.

Calvo Fernandez, N., R. R. Garcia, R. Garcia Herrera, D. Gallego Puyol, L. Gimeno Presa, E. Hernandez Martin, and P. Ribera Rodriguez, 2004: Analysis of the ENSO signal in tropospheric and stratospheric temperatures observed by MSU, 1979 - 2000. *J. Climate*, **17**, 3934-3946, doi:10.1175/1520-0442(2004)017<3934:AOTESI>2.0.CO;2.

Collimore, C. C., D. W. Martin, M. H. Hitchman, A. Huesman and D. E. Waliser, 2003: On the relationship between the QBO and tropical deep convection. *J. Climate*, **16**, 2552-2568.

Eyring, V., and Coauthors, 2006: Assessment of temperature, trace species and ozone in chemistry-climate model simulations of the recent past. *J. Geophys. Res.*, **111**, D22308, doi:10.1029/2006JD007327.

Free, M., and D. J. Seidel, 2009: Observed El Niño-Southern Oscillation temperature signal in the stratosphere. *J. Geophys. Res.*, **114**, D23108, doi:/10.1029/2009JD012420.

Garcia-Herrera, R., N. Calvo, R. R. Garcia, and M. A. Giorgetta, 2006: Propagation of ENSO temperature signals into the middle atmosphere: A comparison of two general circulation models and ERA-40 reanalysis data. *J. Geophys. Res.*, **111**, D06101, doi:10.1029/2005JD006061.

Garfinkel, C. I., and D. L. Hartmann, 2007: Effects of the El Niño-Southern Oscillation and the Quasi-Biennial Oscillation on polar temperatures in the stratosphere. *J. Geophys. Res.*, **112**, D19112, doi:10.1029/2007JD008481.

Garfinkel, C. I., and D. L. Hartmann, 2008: Different ENSO teleconnections and their effects on the stratospheric polar vortex. *J. Geophys. Res.*, **113**, D18114, doi:10.1029/2008JD009920.

Holton, J. R., and H.-C. Tan, 1980: The influence of the equatorial quasi-biennial oscillation on the global circulation at 50mb. *J. Geophys. Res.*, **37**, 2200-2208.

Hurwitz, M. M., P. A. Newman, F. Li, L. D. Oman, O. Morgenstern, P. Braesicke, and J. A. Pyle, 2010: Assessment of the Breakup of the Antarctic Polar Vortex in Two New Chemistry-Climate Models. *J. Geophys. Res.*, **115**, D07105, doi:10.1029/2009JD012788.

Juillet-Leclerc, A., S. Thiria, P. Naveau, T. Delcroix, N. Le Bec, D. Blamart, and T. Corrège, 2006: SPCZ migration and ENSO events during the 20th century as revealed by climate proxies from a Fiji coral. *Geophys. Res. Lett.*, **33**, L17710, doi:10.1029/2006GL025950.

Kanamitsu, M., W. Ekisuzaki, J. Woollen, S.-K. Yang, J. J. Hnilo, M. Fiorino, and G. L. Potter, 2002: NCEP-DOE AMIP-II Reanalysis (R-2). *Bull. Am. Meteorol. Soc.*, **83**, 1631-1643, doi:10.1175/BAMS-83-11-1631(2002)083<1631:NAR>2.3.CO;2.

Kug, J.-S., F.-F. Jin, and S.-I. An, 2009: Two types of El Niño events: cold tongue El Niño and warm pool El Niño. *J. Climate*, **22**, 1499-1515.

Larkin, N.K., and D. E. Harrison, 2005: On the definition of El Niño and associated seasonal average U.S. weather anomalies. *Geophys. Res. Lett.*, **32**, L13705, doi:10.1029/2005GL022738.

Manzini, E., M. A. Giorgetta, M. Esch, L. Kornblueh, and E. Roeckner, 2006: The influence of sea surface temperatures on the Northern winter stratosphere: ensemble simulations with the MAECHAM5 model. *J. Climate*, **19**, 3863-3881.

Newman, P. A., E. R. Nash, and J. E. Rosenfield, 2001: What controls the temperature of the Arctic stratosphere during the spring? *J. Geophys. Res.*, **106**, D17, 19,999-20,010.

Randel, W. J., R. R. García, N. Calvo, and D. Marsh, 2009: ENSO influence on zonal mean temperature and ozone in the tropical lower stratosphere. *Geophys. Res. Lett.*, **36**, L15822, doi:10.1029/2009GL039343.

Rasmusson, E. M., and T. H. Carpenter, 1982: Variation in tropical sea surface temperature and surface wind fields associated with Southern Oscillation/El Niño. *Mon. Weather Rev.*, **110**, 354-384.

Sassi, F., D. Kinnison, B. A. Boville, R. R. Garcia, and R. Roble, 2004: Effect of El Niño-Southern Oscillation on the dynamical, thermal, and chemical structure of the middle

563 atmosphere. *J. Geophys. Res.*, **94**, 14705-14716,
564 doi:10.1029/JD094iD12p14705.
565
566 Taguchi, M., 2010: Wave driving in the tropical lower
567 stratosphere as simulated by WACCM. Part II: ENSO-induced
568 changes for northern winter. *J. Atm. Sci.*, **67**,
569 doi:10.1175/2009JAS3144.1.
570
571 Uppala, S. M., and Coauthors, 2005: The ERA-40 re-analysis. *Q.*
572 *J. R. Meteorol. Soc.*, **131**, 2961-3012, doi:10.1256/qj.04.176.
573
574 Vera, C., G. Silvestri, V. Barros, and A. Carril, 2004:
575 Differences in El Niño response over the Southern Hemisphere. *J.*
576 *Climate*, **17**, 1741-1753.
577
578 Xie, S.-P., C. Deser, G. A. Vecchi, J. Ma, H. Y. Teng, and A. T.
579 Wittenberg, 2010: Global warming pattern formation: sea surface
580 temperature and rainfall. *J. Climate*, **23**, 966-986.
581
582 Yeh, S.-W., B. Y. Yim, Y. Noh, and B. Dewitte, 2009: Changes in
583 mixed layer depth under climate change projections in two CGCMs.
584 *Climate Dynamics*, **33**, 199-213.
585
586 Yu, J.-Y. and S. T. Kim, 2010: Three evolution patterns of
587 Central-Pacific El Niño. *Geophys. Res. Lett.*, **37**, L08706,
588 doi:1029/2010GL042810.
589

589 **Tables & Figures**

590

WPEN	1986	1991	1994	2002	2003	2004	2006	2009				
		*	*		*							
CTEN	1982	1987	1997									
ENSON	1979	1980	1981	1985	1989	1992	1993	1996	2000	2001	2005	2008
	*		*		*			*	*	*	*	

591 **Table 1:** Years classified as WP El Niño (WPEN), CT El Niño
592 (CTEN) and ENSO neutral (ENSON). Classification is based on the
593 SON mean Niño 3 and Niño 4 indices, as described in the text.
594 Events marked with a star symbol coincide with years when the QBO
595 is in its easterly phase.

596

	ERA-40	**MERRA**		**NCEP**	
	1979-2001	***1979-2001***	***1979-2009***	***1979-2001***	***1979-2009***
WPEN	16.55 ± 6.18	15.77 ± 8.02	12.47 ± 7.74	14.54 ± 6.76	11.58 ± 7.06
CTEN	11.41 ± 3.44	11.36 ± 3.48	11.36 ± 3.48	9.93 ± 2.88	9.93 ± 2.88
ENSON	12.22 ± 5.18	11.73 ± 4.12	11.72 ± 3.94	10.82 ± 4.52	10.78 ± 4.24

597 **Table 2:** October/November mean eddy heat flux (K m s^{-1}) at 40-
598 80°S, 100 hPa ± 2 standard deviations for the WP El Niño, CT El
599 Niño and ENSO neutral cases. Years shown in the second row
600 denote SON seasons.

601

		ERA-40	**MERRA**	**NCEP**
WPEN	**QBO-E**	18.28 ± 2.06	16.64 ± 5.10	15.26 ± 4.34
	QBO-W & neutral	13.08	9.97 ± 2.94	8.90 ± 2.58
ENSON	**QBO-E**	11.90 ± 6.78	11.73 ± 5.06	10.62 ± 5.72
	QBO-W & neutral	12.68 ± 1.28	11.71 ± 2.08	11.00 ± 2.58

602 **Table 3:** October/November mean eddy heat flux (K m s^{-1}) at 40-
603 80°S, 100 hPa ± 2 standard deviations for the WP El Niño and ENSO
604 neutral cases. Eddy heat flux is shown as a function of both
605 ENSO and QBO phase.
606
607

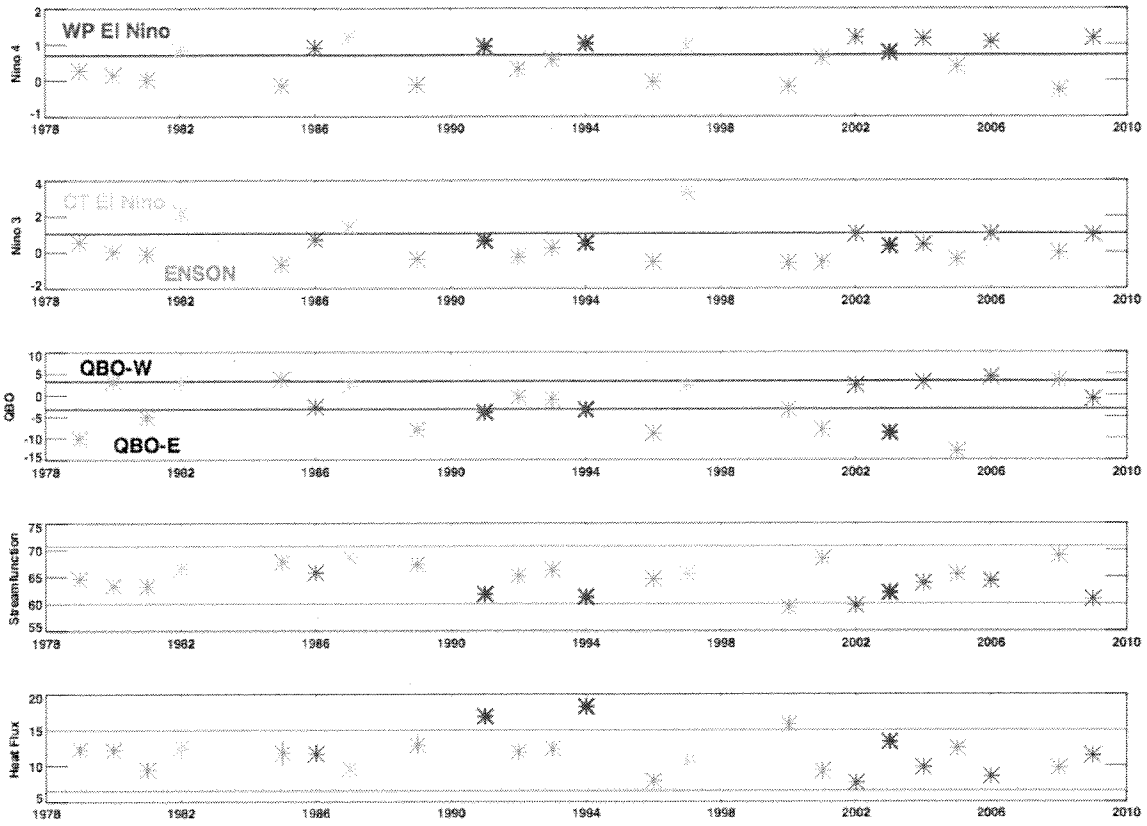

607

608 **Figure 1**: Timeseries showing conditions during El Niño and
609 ENSO neutral events within the 1979-2009 period. Thick (thin)
610 blue stars indicate WP El Nino events coincident with the
611 easterly (westerly or neutral) phase of the QBO. Green stars
612 indicate CT El Niño events. Brown stars indicate ENSO neutral
613 events. The top row shows the SON Niño 3 index (as described in
614 the text); the black line shows the cutoff value defining CT El
615 Niño events. The second row shows the SON Niño 4 index; the
616 black line shows the cutoff value defining WP El Niño events.
617 The third row shows the QBO index (as described in the text);
618 black lines show the cutoff values defining easterly QBO and
619 westerly QBO events. The fourth row shows the average SON
620 streamfunction in the region 210-270°E, 55-75°S (10^{-6} m^3 s^{-1});
621 brown lines indicate ± 2 standard deviations from the mean of
622 ENSO neutral events. The fifth row shows October/November eddy

623 heat flux (K m s^{-1}) at 100 hPa, 40-80°S; brown lines indicate ± 2
624 standard deviations from the mean of ENSO neutral events.

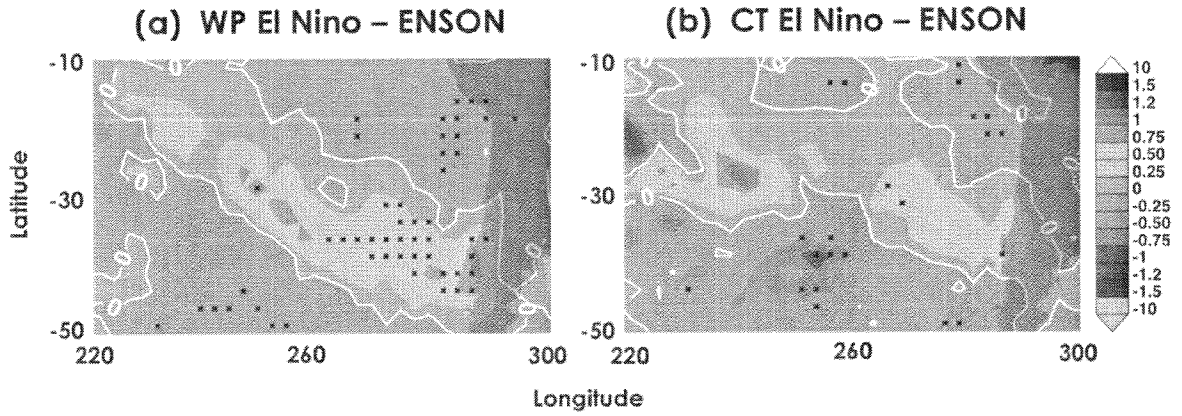

625

626 **Figure 2**: GPCP SON precipitation differences (mm day^{-1}) from a
627 composite of ENSO neutral events, in (a) WP El Niño events and
628 (b) CT El Niño events, in the SPCZ region. White contours
629 indicate zero difference from the composite of ENSO neutral
630 events. Black Xs indicate differences that are significant at
631 the 95% confidence level.

632

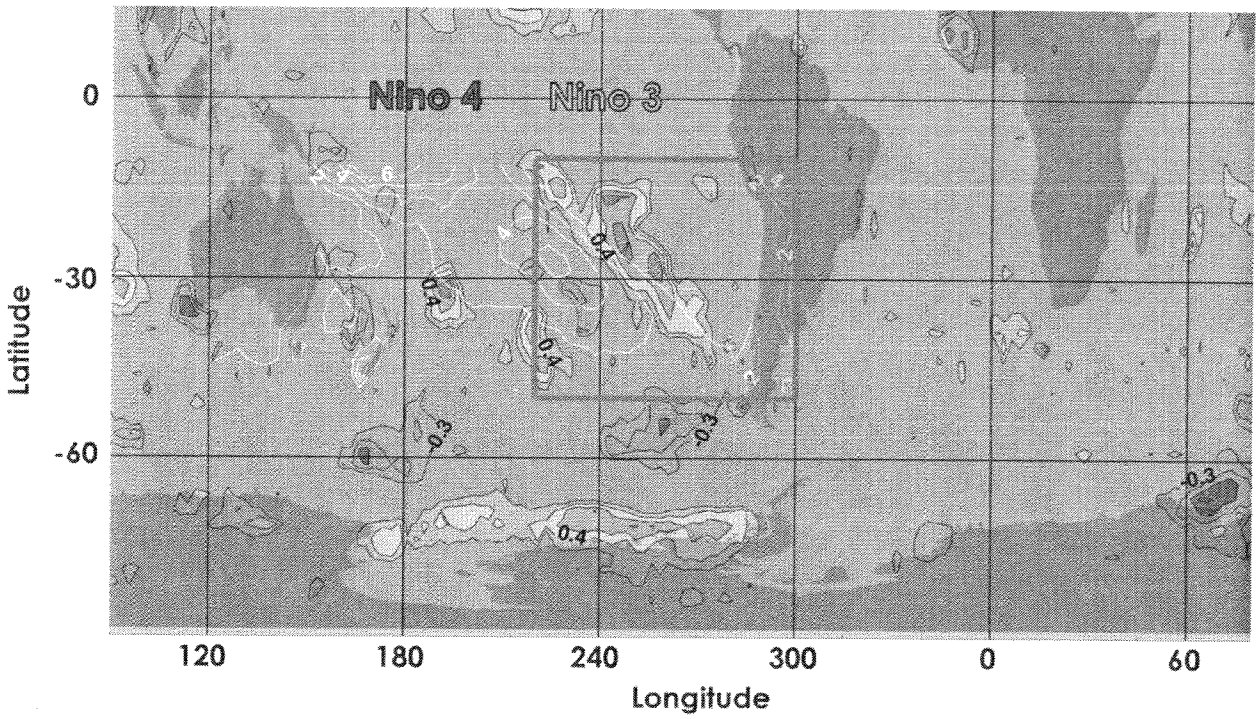

632

633 **Figure 3**: Filled contours show the point correlation between
634 GPCP SON precipitation and NCEP October/November eddy heat flux
635 at 100 hPa, 40-80°S, for the 1979-2007 period. The highest
636 correlation coefficient is 0.69. The SPCZ region, highlighted in
637 Figure 2, is shown as the red box. White contours show
638 climatological mean SON precipitation (mm day^{-1}) in the South
639 Pacific. The locations of the Niño 3 and Niño 4 regions are
640 labeled.

641

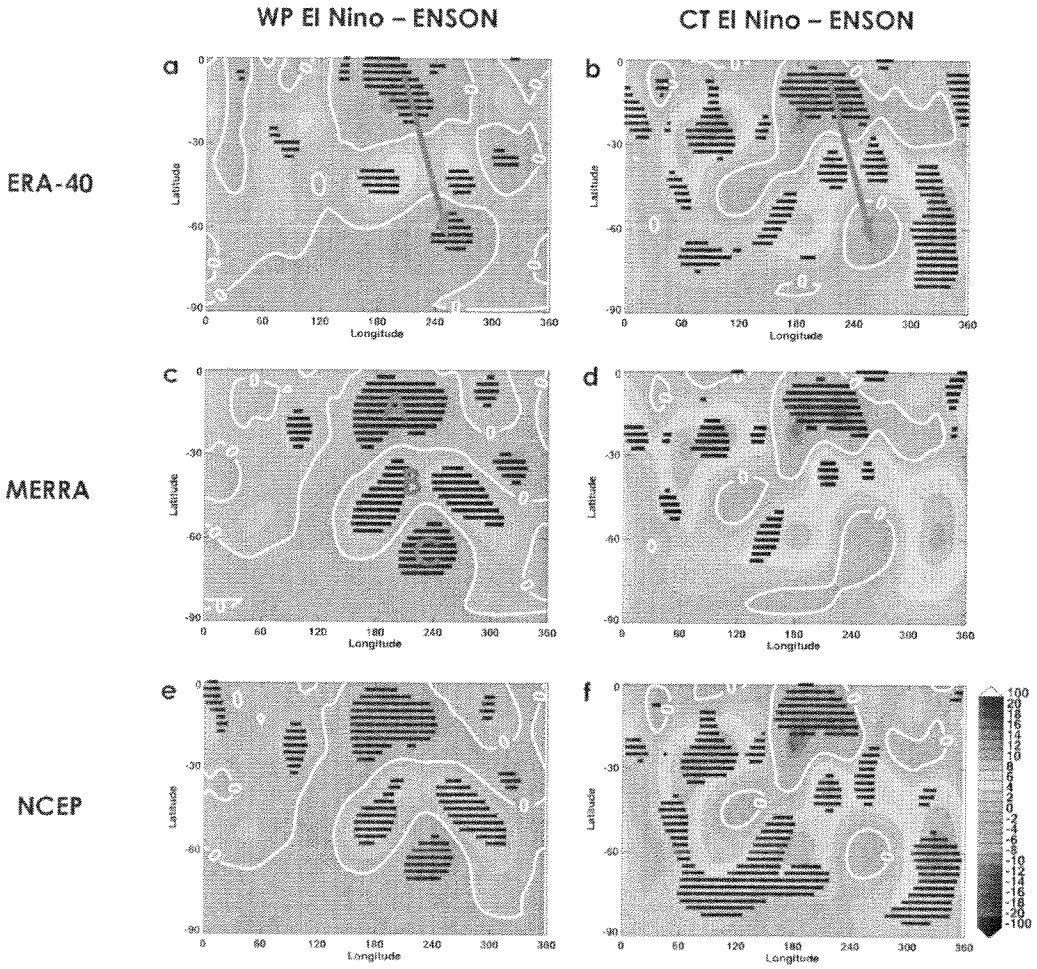

641

642 **Figure 4**: Longitude-latitude contour plots showing SON mean
643 250 hPa streamfunction differences (10^{-6} m^3 s^{-1}), from a composite
644 of ENSO neutral events, in WP El Niño events (a, c, e) and CT El
645 Niño events (b, d, f). White contours indicate zero difference
646 from the composite of ENSO neutral events. Black Xs indicate
647 differences that are significant at the 95% confidence level.
648 Red arrows (a, b) indicate the approximate direction of the
649 planetary wave trains induced by El Niño events. Red letters A,
650 B and C (c) indicate the three regions discussed in the text.
651

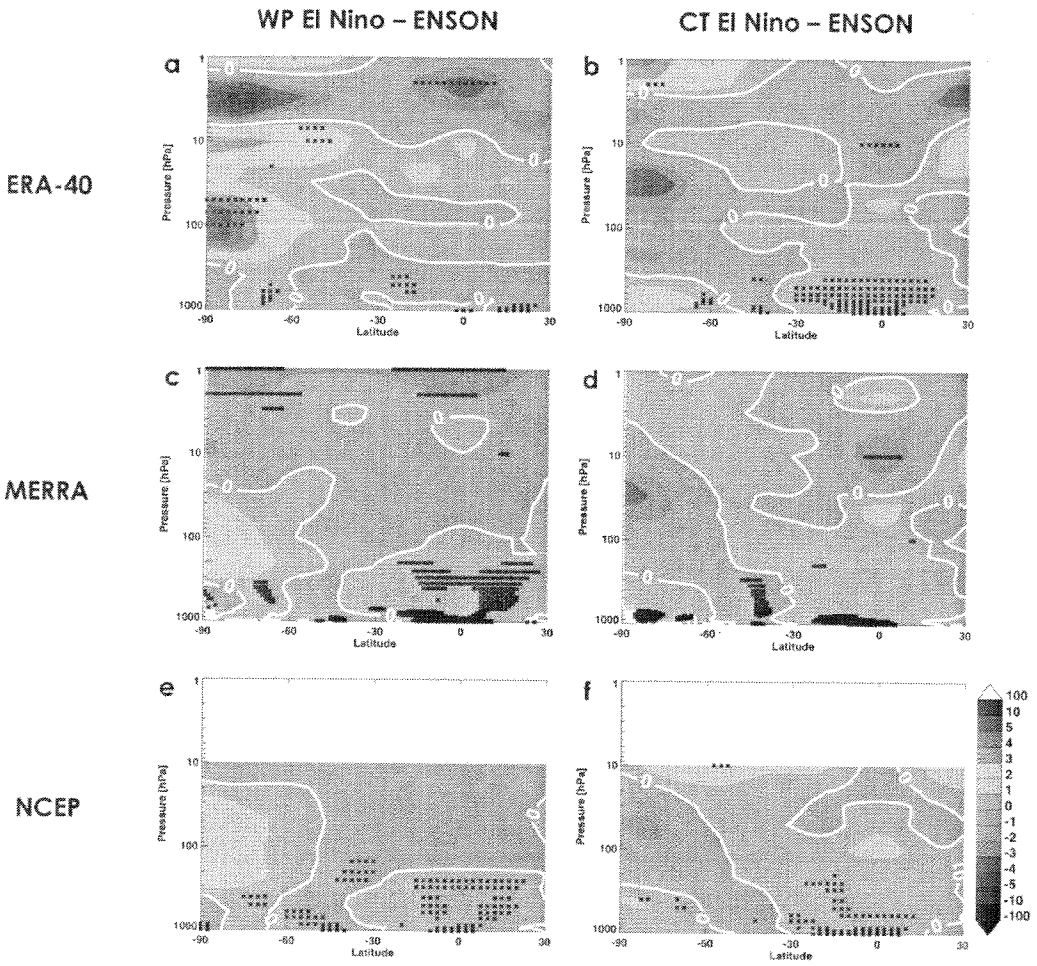

Figure 5: Latitude-height cross-sections of November/December mean temperature differences (K), from a composite of ENSO neutral events, in WP El Niño events (a, c, e) and CT El Niño events (b, d, f). White contours indicate zero difference from the composite of ENSO neutral events. Black Xs indicate differences that are significant at the 95% confidence level.

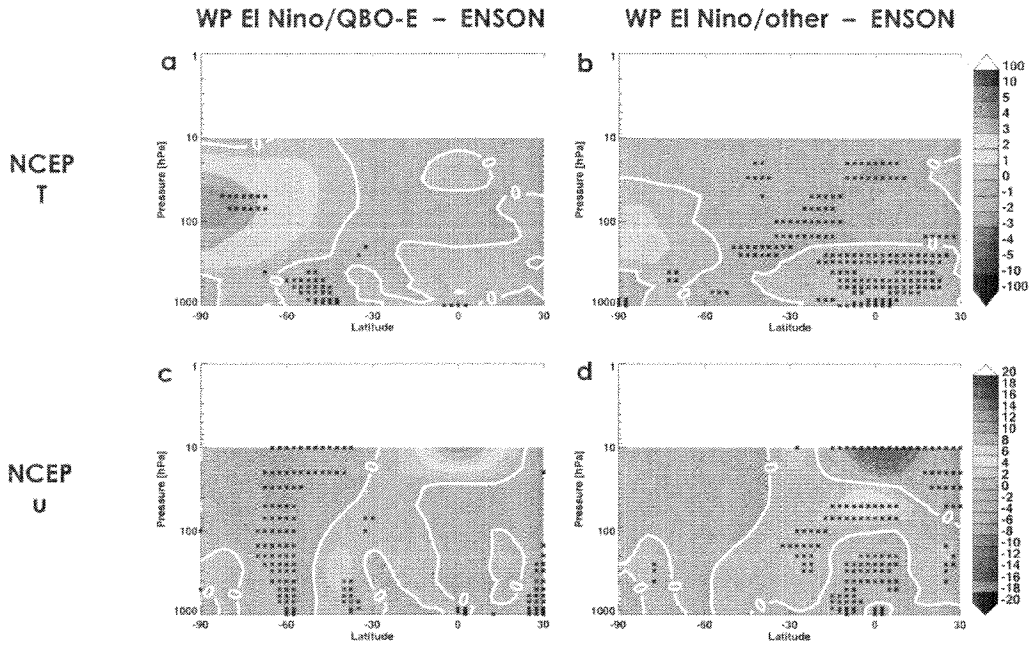

Figure 6: Latitude-height cross-section of November/December mean temperature differences (K) (a, b) and zonal wind differences (m s^{-1}) (c, d), from a composite of ENSO neutral events, in WP El Niño events with easterly QBO (a, c) and WP El Niño events with neutral or westerly QBO (b, d). The NCEP reanalysis is shown. White contours indicate zero difference from the composite of ENSO neutral events. Black Xs indicate differences that are significant at the 95% confidence level.